Nonlinear Vibration and Stability Analysis of Axially Accelerating Beam in Axial Flow

YAN Hao[1,2], NI Qiao[1,2], ZHOU Kun[1,2], DAI Huliang[1,2], WANG Lin[1,2*]

1. School of Aerospace Engineering, Huazhong University of Science and Technology, Wuhan 430074, P.R. China;
2. Hubei Key Laboratory for Engineering Structural Analysis and Safety Assessment, Wuhan 430074, P.R. China

Abstract: The dynamics of an axially accelerating beam subjected to axial flow is studied. Based on the Floquet theory and the Runge-Kutta algorithm, the stability and nonlinear vibration of the beam are analyzed by considering the effects of several system parameters such as the mean speed, flow velocity, axial added mass coefficient, mass ratio, slenderness ratio, tension and viscosity coefficient. Numerical results show that when the pulsation frequency of the axial speed is close to the sum of first- and second-mode frequencies or twice the lowest two natural frequencies, instability with combination or subharmonic resonance would occur. It is found that the beam can undergo the periodic-1 motion under subharmonic resonance and the quasi-periodic motion under combination resonance. With the change of system parameters, the stability boundary may be widened, narrowed or drifted. In addition, the vibration amplitude of the beam under resonance can also be affected by changing the values of system parameters.

Key words: axially accelerating beam; axial flow; subharmonic resonance; combination resonance; Floquet theory

CLC number: O322   **Document code:** A   **Article ID:** 1005-1120(2022)01-0012-11

0 Introduction

In the past decades, the dynamics of axially moving beams have received increasing attention due to their widespread industrial applications, such as aerial cables, power transmission belts and band saw blades. Ulsoy et al.[1], Wickert and Mote[2-3], and Chen[4] have conducted extensive literature reviews on this dynamical system.

In fact, many real mechanisms can be represented by axially moving beams with pulsating or time-dependent velocities, i.e. axially accelerating beams. The nonlinear dynamical behaviors of axially accelerating beam have been studied extensively for many years. Chen and his coworkers[5-10] conducted many studies on the stability and nonlinear dynamics of axially accelerating viscoelastic beams by numerical and analytical methods. Sahoo et al.[11-12] discussed the internal resonance, bifurcation and chaotic dynamics of accelerating beams. Based on

the method of multiple scales, Wang et al.[13] investigated the principal parametric resonance of an axially accelerating hyperelastic beam. Ghayesh[14] numerically calculated the subharmonic dynamics of an axially accelerating beam, showing that the beam can exhibit periodic, quasi-periodic, and chaotic responses with the variation of system parameters such as mean value of the speed. Moreover, some researchers have investigated the nonlinear dynamics of axially accelerating structures modeled by Euler-Bernoulli[15], Rayleigh[16] and Timoshenko beam theories[17].

In many cases, the surrounding fluid can be ignored, as has been done in the aforementioned literature. However, in some special applications such as the steel strip in continuous hot-dip galvanizing process[18-19] and the underwater towed slender structures, the effect of surrounding fluid on the axially moving beam is of great significance. Thus, many investigators have studied the interaction between

the axially moving beam and the fluid. Ni et al.[20] and Li et al.[21] respectively studied the stability and dynamics of axially moving cantilevered beam and supported beams in fluid, showing some rich dynamical behaviors of the beam. Wang and Ni[22] proposed a theoretical model of an axially moving beam immersed in fluid supported by two ends with torsional springs. Their numerical results showed that the beam can lose stability by buckling. Kheiri et al.[23-24] derived three-dimensional linear equations of motion with the consideration of cross flow effect and studied the dynamics of underwater towed long pipes. They concluded that the pipe may lose stability by either divergence or flutter. Taleb et al.[25] and Gosselin et al.[26] studied the dynamics and stability of an axially deploying/extruding beam submerged in dense fluid. Motivated by their work, Yan et al.[27] constructed a theoretical model of an extending beam attached to an axially moving base immersed in dense fluid. The numerical results showed that the moving speed of the base can stabilize the beam. Moreover, Ref.[28] and Ref.[29] respectively studied the linear and nonlinear dynamics of an axially sliding cantilevered pipe conveying fluid.In Refs.[18-29], it was assumed that the beam is immersed in calm fluid, i.e. the axial flow velocity equals to zero. In fact, the case of surrounding fluid flows axially with non-zero velocity is very common in many fields such as ocean engineering. Recently, Yan et al.[30] proposed a simple theoretical model for the dynamical behavior of an axially moving beam subjected to axial flow and derived the nonlinear equation of motion for this system via force balance method. Their numerical results showed that the beam can experience buckling and flutter instabilities with increasing axial moving speed. The effects of flow velocity, slenderness ratio and some other parameters on the instability mode, buckling displacement and flutter amplitude of the beam were explored. In their study, however, they only considered the beam moving with a constant axial speed. In practice, the beam may undergo axially accelerating or decelerating motions in many cases. Motivated by this, we will further expand the existing works by considering an axially accelerating beam with time-varying moving speed.

In this paper, a theoretical model of an axially accelerating beam supported at both ends and subjected to axial flow is established. The nonlinear equation of motion is derived first and then discretized into a set of nonlinear ordinary differential equations via the Galerkin's technique. Based on the Floquet theory and the Runge-Kutta algorithm, the stability and dynamic response of the beam are obtained, and the effects of axially moving speed, flow velocity and several other system parameters on the dynamical behaviors of the beam are analyzed.

1　Problem Formulation

Fig.1 shows a simply-supported beam of length l, diameter D, area moment of inertia I, and mass per unit length m traveling at a time-dependent axial speed $V(t)$ under an applied tension N_0. It is assumed that the beam is made of viscoelastic material of the Kelvin-Voigt model and hence the flexural stiffness of the beam may be written as $E_0 I(1+\gamma \partial/\partial t)$, with E_0 and γ being the Young's modulus and viscoelastic coefficient respectively. In addition, the axially accelerating beam is subjected to an axial flow with density ρ and velocity V_f.
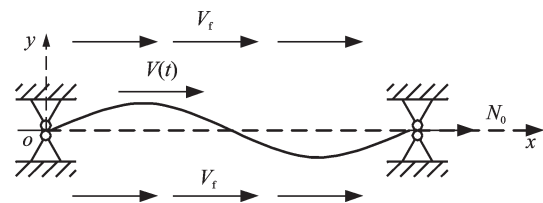
Fig.1　Schematic of an axially accelerating beam in axial flow

The nonlinear equation of motion of the axially moving beam in axial flow has been derived previously by Yan et al.[30], and can be given by the following dimensionless form

$$\eta'''' + \bar{\gamma}\dot{\eta}'''' + \left(\phi v^2 + \beta^2\left(v_f+v\right)^2 + (\phi+\beta)\varphi^{1/2}\dot{v}(1-\xi) - \right.$$
$$\frac{1}{2}c_f\varepsilon\left(v_f-v\right)^2(1-\xi)\,\mathrm{sgn}\left(v_f-v\right) - \Gamma - \frac{\mu}{2}\int_0^1\eta'^2\mathrm{d}\xi -$$
$$\bar{\gamma}\mu\int_0^1\eta'\dot{\eta}'\mathrm{d}\xi\bigg)\eta'' + 2\left((\phi+\beta)v+\beta v_f\right)\varphi^{1/2}\dot{\eta}' +$$
$$\left[\frac{1}{2}\varepsilon\left(c_f\left|v_f-v\right|v_f+\bar{c}_d\varphi^{1/2}v\right)+\beta\varphi^{1/2}\dot{v}_f\right]\eta' + \frac{1}{2}\varepsilon\left(\varphi^{1/2}c_f\left|v_f-\right.\right.$$

$$v \Big| + \bar{c}_d \varphi \Big) \dot{\eta} + \ddot{\eta} = 0 \tag{1}$$

In Eq.(1), several dimensionless quantities and parameters are defined by

$$\eta = \frac{w}{l}, \ \xi = \frac{x}{l}, \ \tau = \sqrt{\frac{E_0 I}{m + m_v}} \frac{t}{l^2} = \alpha t, \ v = \sqrt{\frac{m_v}{E_0 I}} V l,$$

$$v_f = \sqrt{\frac{m_v}{E_0 I}} V_f l, \ \varphi = \frac{m_v}{m + m_v}, \ \phi = \frac{m}{m_v}, \ \varepsilon = \frac{l}{D}, \bar{\gamma} =$$

$$\alpha \gamma, \bar{c}_d = \frac{c_d}{\alpha l}, \ \Gamma = \frac{N_0 l^2}{E_0 I}, \ \mu = \frac{A l^2}{I} = 16 \left(\frac{l}{D}\right)^2 = 16 \varepsilon^2 \tag{2}$$

where $w(x, t)$ and $\eta(\xi, \tau)$ are the dimensional and dimensionless transverse displacement of the beam; the over-dot and the prime denote the derivatives with respect to dimensionless time τ and the coordinate of the centerline of the beam ξ, respectively; v and v_f are the dimensionless axial speed of the beam and the flow velocity, respectively; φ and ϕ are two kinds of mass ratio; β and ε are the axial added mass coefficient and the slenderness ratio, respectively; c_f and c_d are the frictional and the form drag coefficients, respectively; $\bar{\gamma}$ and Γ are the dimensionless viscosity coefficient and tension, respectively; $\text{sgn}(v_f - v)$ in Eq.(1) is a sign function, i. e. $\text{sgn}(v_f - v) = 1$ if $v_f > v$; $\text{sgn}(v_f - v) = -1$ if $v_f < v$, and $\text{sgn}(v_f - v) = 0$ if $v_f = v$. For an accelerating beam, the axial speed v is characterized as a small periodic pulsation on the mean speed v_0, namely

$$v = v_0(1 + a \sin \omega \tau) \tag{3}$$

where a and ω are the dimensionless pulsating amplitude and frequency, respectively.

2 Solution Method

The governing equation can be discretized by applying Galerkin's technique, with the simply-supported beam eigenfunctions $\phi_j(\xi) = \sqrt{2} \sin(j\pi\xi)$ being the admissible functions, thus

$$\eta(\xi, \tau) = \sum_{j=1}^{N} \phi_j(\xi) q_j(\tau) \tag{4}$$

where $q_j(\tau)$ is the corresponding generalized coordinates.

Substituting the expression of Eq.(4) into Eq.(1), multiplying by $\phi_i(\xi)$ and integrating from 0 to 1 leads to

$$M\ddot{q} + C\dot{q} + Kq + N(q) = 0 \tag{5}$$

where M, C, K and N represent the structural mass matrix, damping matrix, stiffness matrix and nonlinear vector, respectively. The elements of these matrices are given by

$$\begin{cases} M_{ij} = e_{ij} = \displaystyle\int_0^1 \phi_i \phi_j \mathrm{d}\xi = \delta_{ij} \\[2mm] N(q) = -\dfrac{\mu}{2} \alpha_{ijkl} q_j q_k q_l - \bar{\gamma}\mu\alpha_{ijkl} q_j q_k \dot{q}_l \\[2mm] C_{ij} = \dfrac{1}{2} \varepsilon\Big[\varphi^{1/2} c_f \big| v_f - v_0(1 + a \sin(\omega\tau)) \big| + \bar{c}_d\varphi \Big] e_{ij} + \\[2mm] \qquad \bar{\gamma}a_{ij} + 2\Big[(\phi + \beta) v_0(1 + a \sin(\omega\tau)) + \beta v_f \Big] \varphi^{1/2} d_{ij} \\[2mm] K_{ij} = a_{ij} + \Big[\phi v_0^2(1 + a \sin(\omega\tau))^2 + \beta^2(v_f + v_0(1 + \\[2mm] \qquad a \sin(\omega\tau)))^2 + \Theta - \Gamma \Big] b_{ij} - \Theta c_{ij} + \Big[\dfrac{1}{2}\varepsilon\big(c_f \big| v_f - \\[2mm] \qquad v_0(1 + a \sin(\omega\tau)) \big| v_f + \bar{c}_d\varphi^{1/2} v_0(1 + \\[2mm] \qquad a \sin(\omega\tau)) \big) + \beta\varphi^{\frac{1}{2}}\dot{v}_f \Big] d_{ij} \end{cases} \tag{6}$$

where

$$\begin{cases} \Theta = (\phi + \beta)\varphi^{1/2} v_0 a\omega\cos(\omega\tau) - \\[2mm] \qquad \dfrac{1}{2} c_f\varepsilon\Big[v_f - v_0(1 + a \sin(\omega\tau)) \Big]^2 \cdot \\[2mm] \qquad \text{sgn}\Big[v_f - v_0(1 + a \sin(\omega\tau)) \Big] \\[2mm] a_{ij} = \displaystyle\int_0^1 \phi_i \phi_j'''' \mathrm{d}\xi = (j\pi)^4 \delta_{ij} \\[2mm] b_{ij} = \displaystyle\int_0^1 \phi_i \phi_j'' \mathrm{d}\xi = -(j\pi)^2 \delta_{ij} \\[2mm] c_{ij} = \displaystyle\int_0^1 \xi\phi_i \phi_j'' \mathrm{d}\xi = \begin{cases} \dfrac{4ij^3}{(j^2 - i^2)^2}\Big[1 - (-1)^{j+i} \Big] & i \neq j \\[3mm] -\dfrac{1}{2}(j\pi)^2 & i = j \end{cases} \\[4mm] d_{ij} = \displaystyle\int_0^1 \phi_i \phi_j' \mathrm{d}\xi = \begin{cases} \dfrac{2ji}{j^2 - i^2}\Big[(-1)^{j+i} - 1 \Big] & i \neq j \\[3mm] 0 & i = j \end{cases} \\[4mm] \alpha_{ijkl} = \displaystyle\int_0^1 \phi_i \phi_j'' \Big|_0^1 \phi_k' \phi_l' \mathrm{d}\xi \mathrm{d}\xi \end{cases} \tag{7}$$

with δ_{ij} being the Kronecker delta function.

Due to the fact that some coefficients of Eq.(5) are time-dependent and periodic, the Floquet theory can be utilized for stability analysis[31]. The Runge-Kutta algorithm will be used to solve Eq.(5) for nonlinear dynamics analysis. Throughout, unless

otherwise specified, a truncation of $N=4$ in the Galerkin's method will be chosen for numerical calculations. The convergence test of the $N=4$ truncation is carried out and the bifurcation diagrams are shown in Figs.2(a,b) for $N=2$, 3 and 4. As can be observed that, $N=4$ is an optimal choice, for the cases of $v_f=3$, $v_0=1$ and $v_f=5$, $v_0=1$.

(a) $v_f=3$, $v_0=1$

(b) $v_f=5$, $v_0=1$
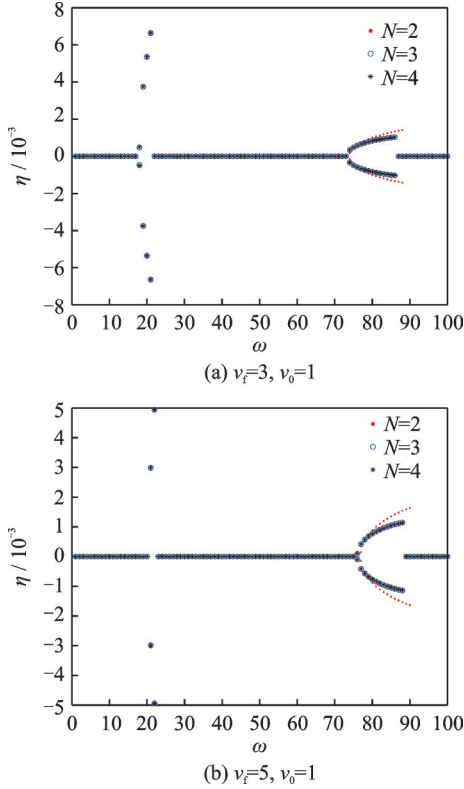
Fig.2   Bifurcation diagrams of beam's responses by using different N

According to Yan et al.[30], several system parameters in the numerical calculation are given by

$$\varphi=0.5, \beta=0.2, \varepsilon=50, a=0.5, \Gamma=1,$$
$$\bar{\gamma}=0.002, \bar{c}_d=0.002, c_f=0.02 \qquad (8)$$

For the sake of simplicity, the over-bar of $\bar{\gamma}$ will not be shown in the following analysis.

3   Results and Discussion

3.1   Stability analysis

In this subsection, Floquet theory is applied to study the stability of the axially accelerating beam system. The effects of several system parameters such as mean speed v_0, flow velocity v_f, axial added mass coefficient β, slenderness ratio ε, mass ratio

φ, tension Γ and viscoelasticity coefficient γ on the stability boundary are analyzed.

Consider an axially accelerating beam subjected to an axial flow with $v_f=5$. The stability boundaries in plane (ω, a) are shown in Fig.3 for $v_0=0.5$, 1 and 1.5. The first two natural frequencies of the beam are calculated by an eigenvalue analysis and given in Table 1. By inspecting the results shown in Fig.3 and Table 1, subharmonic and combination resonances of the first and second modes can be observed in the vicinity of $2\omega_1$, $2\omega_2$ and $\omega_1+\omega_2$ in the case of $v_0=1.5$. However, the combination resonance and the subharmonic resonance of the first mode disappear as v_0 decreases from 1 to 0.5. Moreover, the decrease of v_0 makes the stability boundaries move towards the increasing direction of the pulsating amplitude a, and drift along the positive direction of the pulsating frequency ω in plane (ω, a), which makes the unstable region become narrow. In other words, the smaller mean speed v_0 leads to the lager instability threshold of a for a given ω, and the smaller unstable range of ω for a given a. Thus, one can conclude that the increase in mean speed v_0 makes the beam system more prone to instability.
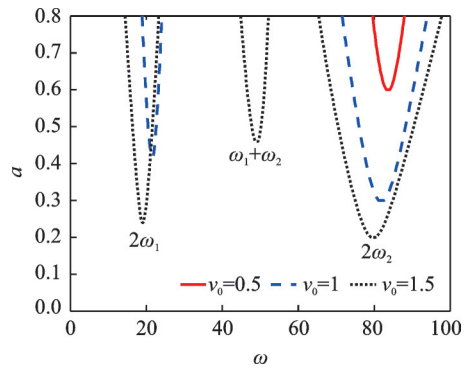
Fig.3   Stability boundaries for various v_0 ($v_f=5$)

Table 1   Natural frequencies of beam for various $v_0(v_f=5)$

v_0	0.5	1	1.5
ω_1	11.73	10.77	9.516
ω_2	41.73	40.86	39.81

Recalling the previous work of Ref.[30], where the problem of an axially moving beam with constant speed in axial flow was considered, it was shown that the beam would lose stability at a critical axial speed $v_{cr}=3.05$ as $v_f=5$ (Fig.3 in Ref.[30]). In this

study, however, it can be seen from Fig.3 that the axially accelerating beam with $v_f = 5$ has the possibility of losing stability via parametric resonance when the axial speed "v" is within the range of [0.5, 1.5] for $a=0.5$ and $v_0=1$, or within the range of [0.2, 0.8] for $a=0.6$ and $v_0 =0.5$. It is obvious that under the same other system parameters, the minimum moving speed for instability of the axially accelerating beam is much lower than that of a beam with constant axially moving speed in Ref.[30].

The influences of v_f, β, ε, φ, Γ and γ on the stability boundaries are presented in Fig.4. As a supplement, Tables 2—7 give the natural frequencies

Table 2 Natural frequencies for beam with different v_f ($v_0=1$)

v_f	0.2	3	5
ω_1	9.684	9.88	10.77
ω_2	39.41	39.76	40.86

Table 3 Natural frequencies for beam with different β ($v_f=3, v_0=1$)

β	0.1	0.3	0.5
ω_1	10.17	9.41	7.857
ω_2	39.94	39.43	38.33

Table 4 Natural frequencies for beam with different ε ($v_f=3, v_0=1$)

ε	30	50	70
ω_1	9.69	9.88	10.06
ω_2	39.57	39.76	39.95

Table 5 Natural frequencies for beam with different φ ($v_f=3, v_0=1$)

φ	0.3	0.4	0.5
ω_1	9.095	9.59	9.88
ω_2	39.22	39.56	39.76

Table 6 Natural frequencies for beam with different Γ ($v_f=3, v_0=1$)

Γ	0	10	20
ω_1	9.38	13.59	16.79
ω_2	39.26	43.96	48.2

Table 7 Natural frequencies for beam with different γ ($v_f=3, v_0=1$)

γ	0.001	0.002	0.003
ω_1	9.882	9.88	9.877
ω_2	39.79	39.76	39.71

of the beam for several typical cases.

The stability boundaries in plane (ω, a) are shown in Fig.4(a) for $v_f=0.2$, 3, 5 and $v_0=1$. In this case, the subharmonic and combination resonances of the first and second modes are observed as $v_f=0.2$ and 3. However, the combination resonance vanishes as v_f increases to 5. In addition, one can also find that the increase of v_f makes the stability boundaries move towards the increasing direction of a and drift slightly along the positive direction of ω in plane (ω, a), which makes the unstable region become narrow. By comparing Fig.3 with Fig.4(a),

(a) $v_0=1$ with different v_f

(b) $v_f=3, v_0=1$ with different β

(c) $v_f=3, v_0=1$ with different ε

(d) $v_f=3, v_0=1$ with different φ

(e) $v_f=3, v_0=1$ with different Γ

(f) $v_f=3, v_0=1$ with different γ
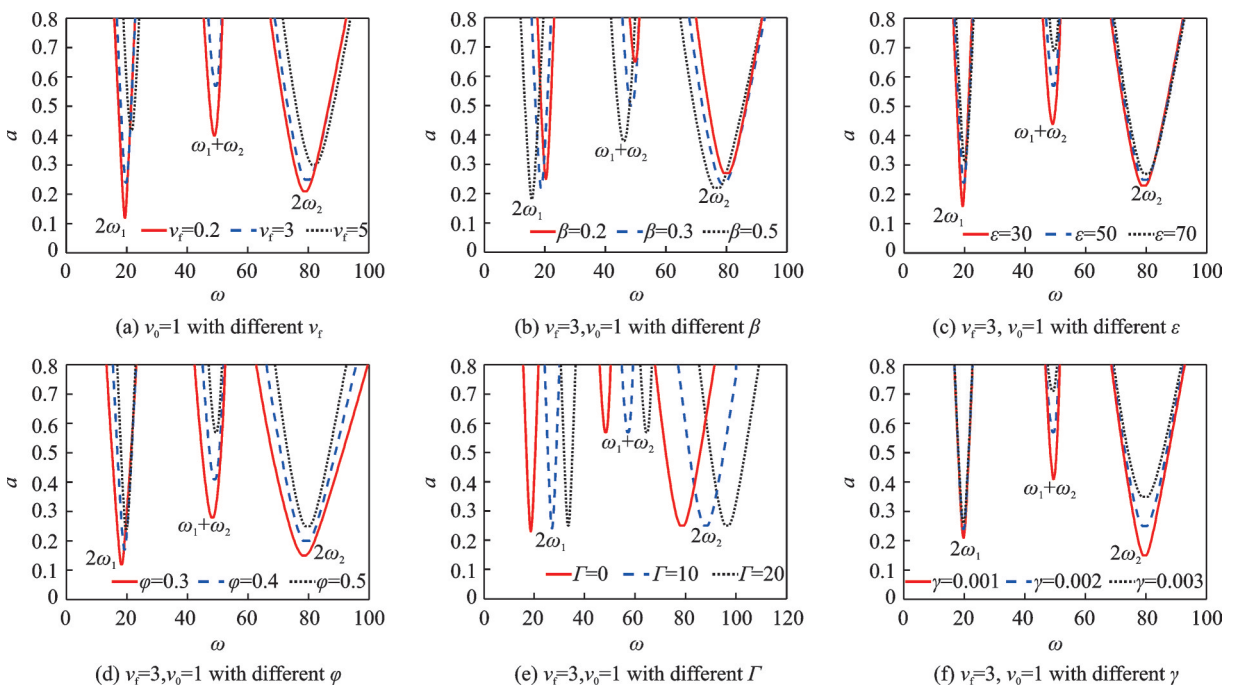
Fig.4 Stability boundaries of beam with different parameters

one can find that the v_0 and v_f have opposite effects on the stability of the beam.

For fixed values of mean axial speed and flow velocity, Figs. 4(b—f) show the stability boundaries of the beam as several parameters are varied, for $v_f=3$ and $v_0=1$. The subharmonic and combination resonances of the first and second modes can be observed. By comparing Figs.4(b—d), it is noted that slenderness ratio ε and mass ratio φ have the same effect on the stability boundaries as v_f. However, the influence of axial added mass coefficient β on the stability boundaries is similar to that of v_0, namely, the decreasing of β makes the stability boundaries moves towards the increasing direction of a and drift along the negative direction of ω in plane (ω, a) and the unstable region becomes narrow.

From Fig. 4(e), it is found that the effect of tension Γ is mainly reflected in making the unstable region drift to the left when Γ is decreased. That means that the increase of Γ would make the stability boundaries move towards the increasing direction of ω. However, the size of the unstable region in plane (ω, a) does not change much. On the contrary, the viscoelasticity coefficient γ can change the size of the unstable region in plane (ω, a), while it has little effect on the shift of the stability boundaries, as can be seen from Fig. 4(f). It is also noted that the presence of γ can enhance the stability of the beam system.

What's more, these figures shown above indicate that the stability boundary for the summation resonance is most sensitive to the change of all system parameters discussed.

3. 2　Nonlinear dynamic analysis

According to the linear stability analysis, it is noted that the beam can experience subharmonic and combination resonances as a and ω vary. To further understand the dynamical behaviors of the beam at resonance, the vibration responses of the beam at resonance are investigated by a nonlinear dynamic analysis in this subsection.

In the nonlinear dynamic analysis, attention is concentrated on the vibrations of the midpoint of the beam ($\xi=0.5$). Effects of system parameters on the vibration responses of the beam can be summarized in the form of bifurcation diagrams, by recording the amplitude of the beam whenever the vibration velocity at $\xi=0.5$ becomes zero.

Fig.5 shows several bifurcation diagrams of the beam's responses for different values of mean speed v_0 and pulsating amplitude a. As can be seen from Fig. 5(a), for $v_f=5$ and $a=5$, the beam remains stable within the ω range of $[0, 100]$ for $v_0=0.5$. However, the beam would lose stability in some ω ranges as v_0 increases to 1 or 1.5. Recalling the stability boundaries shown in Fig.3, it can be seen that when $v_0=1.5$, the beam suffers, respectively, a first-mode subharmonic resonance, a combination resonance and a second-mode subharmonic resonance in the ω ranges of $[16.4, 21.6]$, $[47.8, 50.2]$ and $[70.5, 90.4]$. When $v_0=1$, the first-mode and second-mode subharmonic resonances occur, respectively in the ω ranges of $[20.4, 22.6]$ and $[76, 88.2]$.

In order to analyze the vibration mechanism of the beam at resonance, phase portraits, Poincaré maps and power-spectrum-density (PSD) diagrams are utilized here as powerful techniques in distinguishing chaotic responses from periodic or quasi-periodic motions.

For $v_f=5$ and $v_0=1.5$, the cases of $\omega=20$ and 49 are chosen as two typical samples for the beam at subharmonic and combination resonances. In the case of $\omega=20$, the phase portrait shown in Fig.6(a1) presents only a limit cycle, the Poincaré map shows a pair of symmetrical points (Fig.6(a2)), and the PSD curve is clear with several obvious peaks and a limited frequency bandwidth (Fig.6(a3)). These results indicate that the beam undergoes a periodic motion. According to Païdoussis[32], the Poincaré map consists of a number of points equal to twice the period number when the motion is periodic. Thus, the beam definitely undergoes a periodic-1 motion when $\omega=20$. As for the case of $\omega=49$, one can find that a limited number of cycles are contained in the phase portrait (Fig.6(b1)), and a series of

points forming a circle are displayed in the Poincaré map (Fig.6(b2)). By inspecting Fig.6(b3) further, the PSD curve has several peaks and a broader frequency bandwidth. Thus, we can point out that the beam undergoes a quasi-periodic motion when $\omega=49$.

Compared with a beam with constant axially moving speed, once the axially accelerating beam becomes unstable, oscillation rather than statically buckling would occur. This is because that parametric resonance is the preferred form of instability of the axially accelerating beam, showing the most important difference between the dynamical system and that of Ref.[30].

Indeed, based on more extensive calculations, it is found that the phase portraits, Poincaré maps and PSD diagrams for several other pulsating frequencies in the resonance ranges are similar to the results of Fig.6. Thus we can conclude that the beam would undergo periodic-1 and quasi-periodic motions in subharmonic resonance and the combination resonance, respectively.

A slightly different bifurcation diagram of Fig.5 (b) is constructed for the beam with $v_f=3$, $v_0=1$ and $a=0.4$, 0.5, 0.6. Results show that the beam loses stability in the ω ranges of [18.5, 21] and [74.9, 84.8] for $a=0.4$; in the ω ranges of [18, 21.5] and [73.2, 86.8] for $a=0.5$; in the ω ranges of [17.6, 21.9], [48.6, 50.2] and [73.2, 86.8] for $a=0.5$. These ω ranges for unstable behavior of the beam are consistent with the results in the linear stability analysis.

From Fig.5, one can also find that the overall vibration amplitude of the beam at resonance increases with the increase of v_0, a and ω.

Effects of v_f, β, ε, φ, Γ and γ on the vibration response of the beam are summarized via bifurcation diagrams presented in Fig.7. It should be noted that all the values of system parameters are chosen to be the same as those defined in Fig.4. Due to the fact that the effects of these parameters on the ω ranges for the beam's instability are consistent with that obtained in the linear stability analysis, only the vibration amplitudes of the beam will be focused on. Figs.7(c, d) show the bifurcation diagrams of the beam for different values of ε and φ, respectively. Both figures show that the larger the values of these two parameters are, the smaller the amplitudes of the beam at resonance become. It can be found from Fig.7(b) that increasing β can increase the vibration amplitude of the beam. And the increase of Γ can increase the vibration amplitude of the beam at the first-mode subharmonic resonance and slightly reduce the amplitude of the beam at the second-mode subharmonic resonance, which can be observed in Fig.7(e). Comparing Figs.7(a, f), it is noted that v_f and γ have the same effect on the vibration amplitude, i.e., increasing v_f or γ can reduce the amplitude of the beam at the first-mode subharmonic resonance and accelerate the growth rate of the vibration amplitude of the beam with increasing ω in the second-mode subharmonic resonance region.
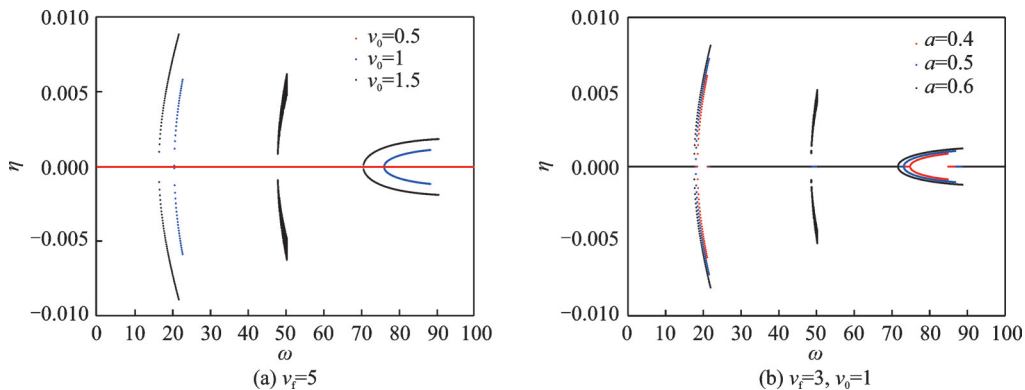
Fig.5   Bifurcation diagrams of beam's responses

(a1) Phase portrait

(a2) Poincaré map

(a3) PSD diagram

(a) ω=20

(b1) Phase portrait

(b2) Poincaré map

(b3) PSD diagram

(b) ω=49

Fig.6   Phase portraits，Poincaré maps and PSD diagrams for $v_f = 5$ and $v_0 = 1.5$

$\cdot v_f$=0.2 $\cdot v_f$=2 $\cdot v_f$=5

(a) v_0=1 with different v_f

$\cdot \beta$=0.1 $\cdot \beta$=0.3 $\cdot \beta$=0.5

(b) v_f=3，v_0=1 with different β

$\cdot \varepsilon$=30 $\cdot \varepsilon$=50 $\cdot \varepsilon$=70

(c) v_f=3，v_0=1 with different ε

$\cdot \varphi$=0.3 $\cdot \varphi$=0.4 $\cdot \varphi$=0.5

(d) v_f=3，v_0=1 with different φ

$\cdot \varGamma$=0 $\cdot \varGamma$=10 $\cdot \varGamma$=20

(e) v_f=3，v_0=1 with different $\varGamma$

$\cdot \gamma$=1e-3 $\cdot \gamma$=2e-3 $\cdot \gamma$=3e-3

(f) v_f=3，v_0=1 with different γ
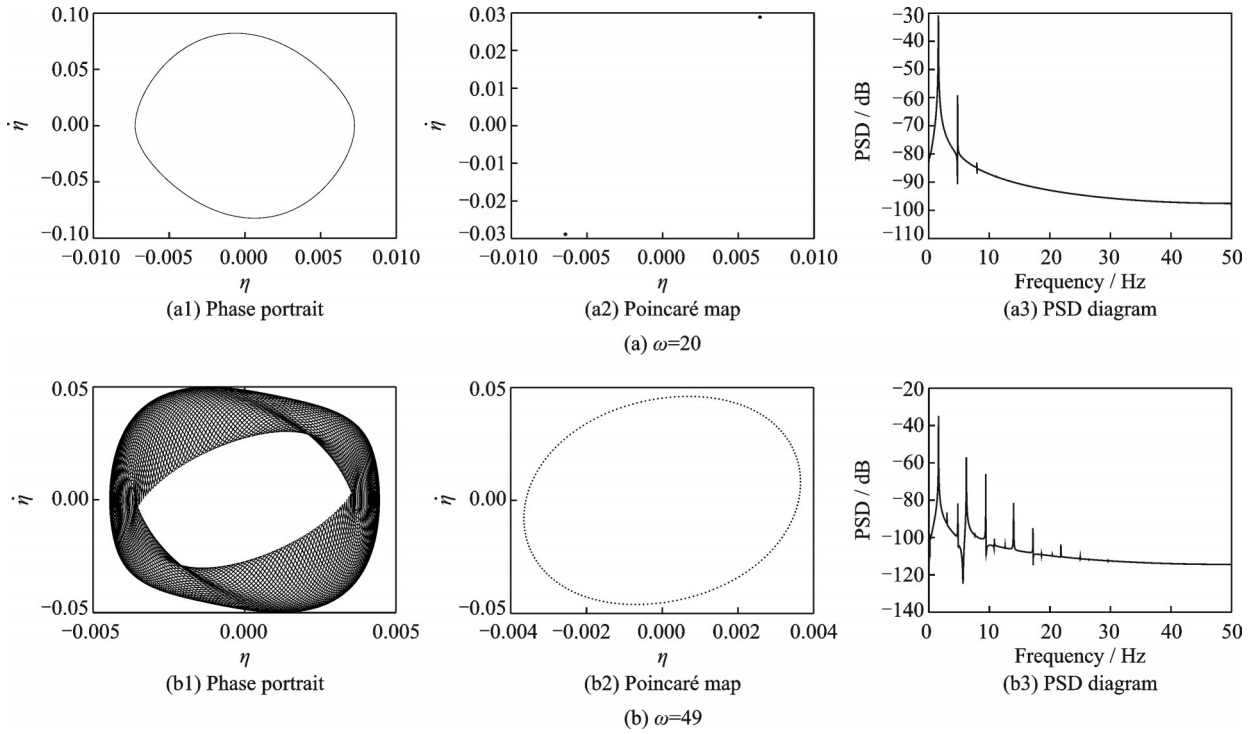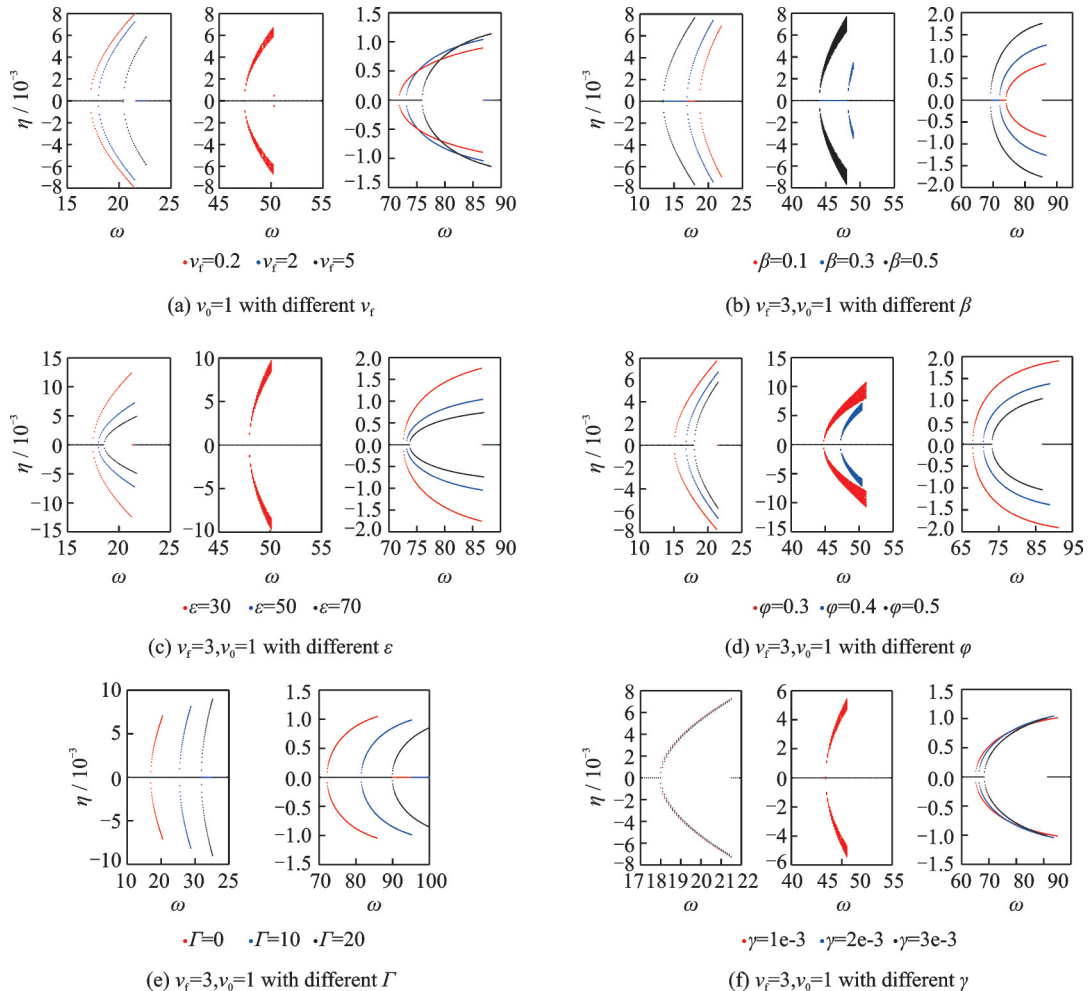
Fig.7   Bifurcation diagrams of beam's responses with different system parameters

4 Conclusions

A theoretical analysis of axially accelerating beams in axial flow has been conducted. The stability and nonlinear dynamic analyses are conducted by Floquet theory and Runge-Kutta algorithm, respectively. Extensive numerical calculations are conducted to analyze the effects of several system parameters such as mean axial speed, flow velocity, axial added mass coefficient, mass ratio, slenderness ratio, tension and viscosity coefficient on the stability and vibration response of the beam.

In the stability analysis, results show that the beam can occur first-mode and second-mode subharmonic resonances in the vicinity of twice the lowest two natural frequencies respectively, and combination resonance in the vicinity of the sum of first- and second-mode frequencies. Effects of several system parameters on the stability boundaries can be summarized as follows:

(1) Increasing the mean speed and axial added mass coefficient can widen the instability regions.

(2) The increase of flow velocity, slenderness ratio, mass ratio, tension and viscoelasticity coefficient can narrow the instability regions.

(3) The stability boundaries can shift along the axis of pulsating frequency as some parameters (except viscoelasticity coefficient) vary.

(4) The stability boundary for the summation resonance is most sensitive to the change of all system parameters.

In the nonlinear dynamic analysis, the conclusion can be drawn out that the beam undergoes periodic-1 and quasi-periodic motions at subharmonic resonance and combination resonance, respectively. Results also show that the vibration amplitude of the beam at resonance can be affected by several key system parameters. Generally speaking, the vibration amplitude would increase with the increase of axial added mass coefficient and pulsating frequency but decreases with the increase of slenderness ratio and mass ratio. However, the increase of flow velocity and viscoelasticity coefficient can reduce the amplitude of the beam at the first-mode subharmonic resonance. Moreover, increasing the tension can increase the vibration amplitude of the beam at the first-mode subharmonic resonance and slightly reduce the amplitude of the beam at the second-mode subharmonic resonance.

References

[1] ULSOY A G, MOTE JR C D, SZYMNI R. Principal developments in band saw vibration and stability research[J]. Holzals Rohund Werkstoff, 1978, 36: 273-280.

[2] WICKERT J A, MOTE JR C D. Current research on the vibration and stability of axially-moving materials[J]. The Shock Vibration Digest, 1988, 20(5): 3-13.

[3] WICKERT J A, MOTE JR C D. Classical vibration analysis of axially moving continua[J]. Journal of Applied Mechanics, 1990, 57(3): 738-744.

[4] CHEN Liqun. Analysis and control of transverse vibrations of axially moving strings[J]. Applied Mechanics Reviews, 2005, 58(2): 91-116.

[5] CHEN Liqun, YANG Xiaodong. Steady-state response of axially moving viscoelastic beams with pulsating speed: Comparison of two nonlinear models[J]. International Journal of Solids Structures, 2005, 42(1): 37-50.

[6] CHEN Liqun, YANG Xiaodong. Transverse nonlinear dynamics of axially accelerating viscoelastic beams based on 4-term Galerkin truncation[J]. Chaos, Solitons & Fractals, 2006, 27(3): 748-757.

[7] CHEN Liqun, YANG Xiaodong. Stability in parametric resonance of axially moving viscoelastic beams with time-dependent speed[J]. Journal of Sound Vibration, 2005, 284(3/4/5): 879-891.

[8] DING Hu, CHEN Liqun. Stability of axially accelerating viscoelastic beams: Multi-scale analysis with numerical confirmations[J]. European Journal of Mechanics—A/Solids, 2008, 27(6): 1108-1120.

[9] DING Hu, CHEN Liqun. Nonlinear dynamics of axially accelerating viscoelastic beams based on differential quadrature[J]. Acta Mechanica Solida Sinica, 2009, 22(3): 267-275.

[10] CHEN L H, ZHANG W, YANG F H. Nonlinear dynamics of higher-dimensional system for an axially accelerating viscoelastic beam with in-plane and out-of-plane vibrations[J]. Journal of Sound & Vibration, 2010, 329(25): 5321-5345.

[11] SAHOO B, PANDA L N, POHIT G. Combination, principal parametric and internal resonances of an accel-

erating beam under two frequency parametric excitation[J]. International Journal of Non-linear Mechanics, 2016, 78: 35-44.

[12] SAHOO B. Bifurcations and chaotic dynamics of an axially accelerating hinged-clamped viscoelastic beam[J]. Iranian Journal of Science and Technology: Transactions of Mechanical Engineering, 2021, 45 (1): 23-41.

[13] WANG Yuanbin, DING Hu, CHEN Liqun. Nonlinear vibration of axially accelerating hyperelastic beams[J]. International Journal of Non-linear Mechanics, 2018, 99: 302-310.

[14] GHAYESH M H. Subharmonic dynamics of an axially accelerating beam[J]. Archive of Applied Mechanics, 2012, 82(9): 1169-1181.

[15] PAKDEMIRLI M, ÖZ H R. Infinite mode analysis and truncation to resonant modes of axially accelerated beam vibrations[J]. Journal of Sound and Vibration, 2018, 311(3/4/5): 1052-1074.

[16] WANG Bo. Effect of rotary inertia on stability of axially accelerating viscoelastic Rayleigh beams[J]. Applied Mathematics Mechanics, 2018, 39(5): 717-732.

[17] TANG Youqi, CHEN Liqun, YANG Xiaodong. Parametric resonance of axially moving Timoshenko beams with time-dependent speed[J]. Nonlinear Dynamics, 2009, 58(4): 715-724.

[18] LI Jian, GUO X H, LUO J, et al. Analytical study on inherent properties of a unidirectional vibrating steel strip partially immersed in fluid[J]. Shock & Vibration, 2013, 20(4): 793-807.

[19] WANG Yanqing, HUANG Xiaobo, LI Jian. Hydroelastic dynamic analysis of axially moving plates in continuous hot-dip galvanizing process[J]. International Journal of Mechanical Sciences, 2016, 110: 201-216.

[20] NI Qiao, LI Mingwu, TANG Min, et al. Free vibration and stability of a cantilever beam attached to an axially moving base immersed in fluid[J]. Journal of Sound & Vibration, 2014, 333(9): 2543-2555.

[21] LI Mingwu, NI Qiao, WANG Lin. Nonlinear dynamics of an underwater slender beam with two axially moving supports[J]. Ocean Engineering, 2015, 108: 402-415.

[22] WANG Lin, NI Qiao. Vibration and stability of an axially moving beam immersed in fluid[J]. International Journal of Solids & Structures, 2008, 45(5): 1445-1457.

[23] KHEIRI M, PAÏDOUSSIS M P, AMABILI M, et al. Three-dimensional dynamics of long pipes towed underwater. Part 1: The equations of motion[J]. Ocean Engineering, 2013, 64: 153-160.

[24] KHEIRI M, PAÏDOUSSIS M P, AMABILI M, et al. Three-dimensional dynamics of long pipes towed underwater. Part 2: Linear dynamics[J]. Ocean Engineering, 2013, 64: 161-173.

[25] TALEB I, MISRA A. Dynamics of an axially moving beam submerged in a fluid[J]. Journal of Hydronautics, 1981, 15(1): 62-66.

[26] GOSSELIN F, PAÏDOUSSIS M P, MISRA A. Stability of a deploying/extruding beam in dense fluid[J]. Journal of Sound and Vibration, 2007, 299(1/2): 123-142.

[27] YAN Hao, NI Qiao, DAI Huliang, et al. Dynamics and stability of an extending beam attached to an axially moving base immersed in dense fluid[J]. Journal of Sound and Vibration, 2016, 383: 364-383.

[28] HUO Yinlei, WANG Zhongmin. Dynamic analysis of a vertically deploying/retracting cantilevered pipe conveying fluid[J]. Journal of Sound and Vibration, 2016, 360: 224-238.

[29] YAN Hao, DAI Huliang, NI Qiao, et al. Nonlinear dynamics of a sliding pipe conveying fluid[J]. Journal of Fluids and Structures, 2018, 81: 36-57.

[30] YAN Hao, DAI Huliang, NI Qiao, et al. Dynamics and stability analysis of an axially moving beam in axial flow[J]. Journal of Mechanics of Materials Structures, 2020, 15(1): 37-60.

[31] NAYFEH A H, MOOK D T, HOLMES P. Nonlinear oscillations[M].[S.l.]: John Wiley & Sons, 1980.

[32] PAÏDOUSSIS M P, LI G X, MOON F C. Chaotic oscillations of the autonomous system of a constrained pipe conveying fluid[J]. Journal of Sound and Vibration, 1989, 135(1): 1-19.

Authors   Dr. **YAN Hao** received the Ph.D. degree in solid mechanics at Huazhong University of Science and Technology, Wuhan, China, in 2019. He is currently a postdoc of School of Aerospace Engineering, Huazhong University of Science and Technology, Wuhan, China. His research is focused on pipe conveying fluid, axially moving structures and nonlinear dynamics.

Prof. **WANG Lin** is currently a full professor of School of Aerospace Engineering, Huazhong University of Science

（Production Editor：SUN Jing）

受轴向外流作用的轴向变速运动梁非线性振动及稳定性分析

严　浩[1,2]，倪　樵[1,2]，周　坤[1,2]，代胡亮[1,2]，王　琳[1,2]

（1.华中科技大学航空航天学院,武汉 430074,中国；

2.工程结构分析与安全评定湖北省重点实验室,武汉 430074,中国）

摘要：研究了受轴向流作用的轴向变速梁的稳定性和动力学特性。利用 Floquet 理论和 Runge-Kutta 算法,得到了轴向变速运动梁动力学响应的数值结果。通过参数分析研究了平均脉动速率、轴向外流速、轴向附加质量参数、质量比、长细比、初始拉力和粘弹性系数等系统参数对梁动力学的影响。研究结果表明,当梁运动速率的脉动频率接近一、二阶固有频率的2倍或前两阶固有频率之和时,轴向运动梁会出现次谐波共振或组合共振现象而失去稳定。梁在次谐波共振区和一、二阶组合共振区内分别做单周期和概周期运动。梁的稳定区域在各系统参数的作用下将出现扩大、收缩和平移的现象。此外,梁共振时的振动幅值同样受到各系统参数的影响。

关键词：轴向变速运动梁;轴向流;次谐波共振;组合共振;Floquet 理论